Angewandte Chemie
Eine Zeitschrift der Gesellschaft Deutscher Chemiker

Supporting Information

Electronic Energy Transfer Modulation in a Dynamic Foldaxane: Proof-of-Principle of a Lifetime-Based Conformation Probe

Sergey A. Denisov, Quan Gan, Xiang Wang, Luca Scarpantonio, Yann Ferrand, Brice Kauffmann, Gediminas Jonusauskas, Ivan Huc, and Nathan D. McClenaghan**

anie_201508611_sm_miscellaneous_information.pdf

Contents

Synthetic schemes

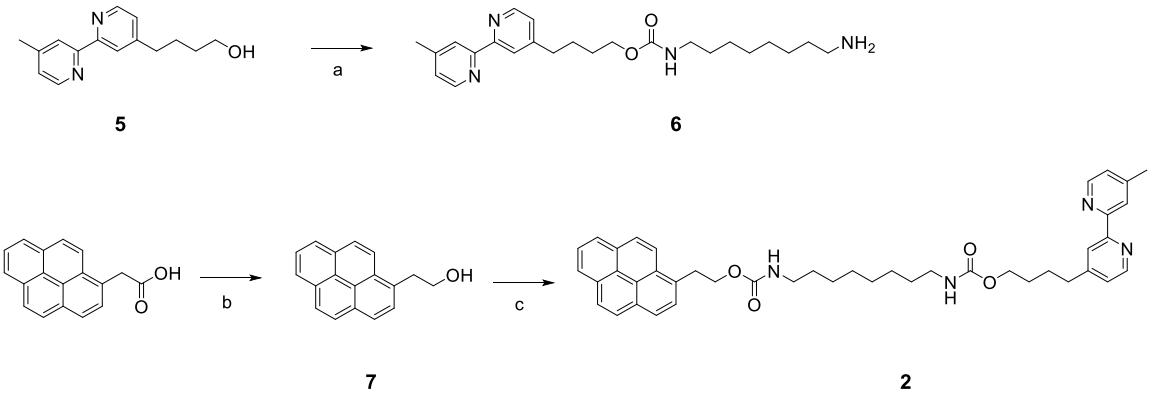

Scheme S1. Synthesis of guest **2**. a) 4-nitrophenyl chloroformate, DIEA, DCM, rt, 3 h, then 1,8-diaminooctane, rt,12 h, (78%); b) $LiAlH_4$, THF, rt, 6 h, (92%); c) 4-nitrophenyl chloroformate, DIEA, chloroform, rt, 3 h, then compound **6**, reflux, 24 h, (65%).

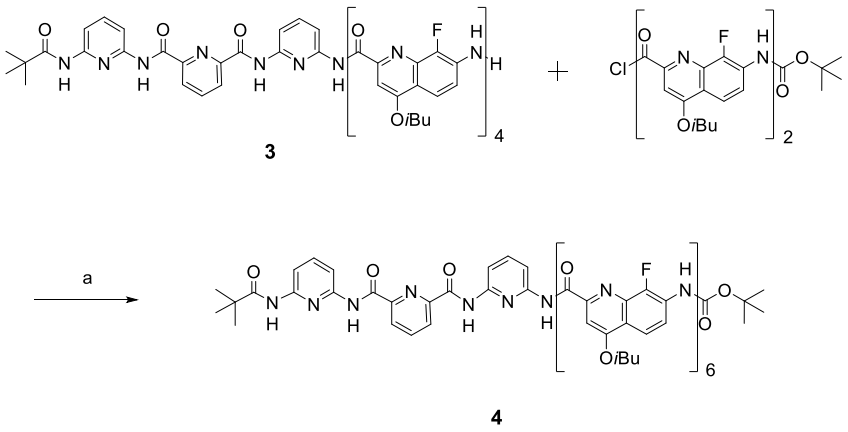

Scheme S2. Synthesis of sequence **4** $\mathbf{P_3Q^F_6}$. a) DIEA, DCM, rt, (83%).

Experimental section

All reactions were carried out under a dry nitrogen atmosphere. Commercial reagents were purchased from Sigma-Aldrich or Alfa-Aesar and were used without further purification unless otherwise specified. Tetrahydrofuran (THF) and dichloromethane (DCM) were dried over alumina; chloroform ($CHCl_3$) and diisopropylethylamine (DIEA) were distilled from calcium hydride (CaH_2) prior to use. Reactions were monitored by thin layer chromatography (TLC) on Merck silica gel 60-F254 plates and observed under UV light. Column chromatography was carried out on Merck GEDURAN Si60 (40-63 µm. ESI mass spectra were obtained on a Waters LCT from the IMAGIF CNRS Laboratory at the Gif/Yvette, France. NMR spectra were recorded on 2 different NMR spectrometers: (1) an Avance II NMR spectrometer (Bruker Biospin) with a vertical 7.05 T narrow-bore / ultrashield magnet operating at 300 MHz for ^1H observation and 75 MHz for ^{13}C observation by means of a 5-mm direct BBO H/X probe with Z gradient capabilities; (2) a DPX-400 NMR spectrometer (Bruker Biospin) with a vertical 9.4 T narrow-bore / ultrashield magnet operating at 400 MHz for ^1H observation by means of a 5-mm direct QNP ^1H / ^{13}C / ^{31}P / ^{19}F probe with gradient capabilities. Chemical shifts are reported in parts per million (ppm, δ) relative to the ^1H residual signal of the deuterated solvent used. ^1H NMR splitting patterns with observed first-order coupling are designated as singlet (s), doublet (d), triplet (t), or quartet (q). Coupling constants (*J*) are reported in hertz. Samples were not degassed. Data processing was performed with Topspin 2.0 software.

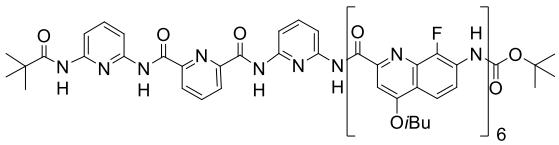

4

Nonamer 4 $P_3Q^F_6$. Heptamer[1] $P_3Q^f_4$ amine (147 mg, 0.1 mmol) and DIEA (0.03 mL, 0.4 mmol) were dissolved in dry CH_2Cl_2 (10 mL), and freshly prepared dimer acid chloride[2] (98 mg, 0.15 mmol) in CH_2Cl_2 (5 mL) was added dropwise at RT. After stirring overnight, solvents were was evaporated and the product was purified by flash chromatography (SiO_2) eluting with cyclohexane/EtOAc (70:30, vol/vol) to obtain **4** as a white solid (0.17 g, 83%). ^1H NMR (d_6-DMSO, 400 MHz, 353 K): δ 11.44 (s, 1H), 10.97 (s, 1H), 10.53 (s, 1H), 10.41 (s, 1H), 10.12 (s, 2H), 9.85 (s, 1H), 9.80 (s, 1H), 8.46 (s, 1H), 8.30 (t, *J*(H, H) = 7.6, 1H), 8.09-7.87 (m, 3H), 7.68-7.21 (m, 15H), 7.03-6.61 (m, 8H), 4.31-3.92 (m, 12H), 2.45-2.26 (m, 6H), 1.42-1.18 (m, 36H), 1.05 (s, 9H), 0.46 (s, 9H), . HRMS (ESI): *m/z* calcd for $C_{111}H_{110}F_6N_{19}O_{17}$ $[2M+2H]^{2+}$ 2094.8231; found 2094.8175.

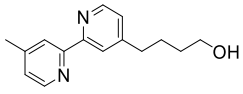

5

2-(4-Methyl-2-pyridinyl)-4-pyridine butanol[3] **5**

^{1}H NMR ($CDCl_3$, 300 MHz): δ 8.57 (d, *J*(H, H) = 4.8, 1H), 8.54 (d, *J*(H, H) = 4.8, 1H), 8.23 (s, 2H), 7.15 (d, *J*(H, H) = 4.8, 1H), 7.15 (d, *J*(H, H) = 4.8, 1H), 3.71-3.65 (m, 2H), 2.77 (t, *J*(H, H) = 7.8, 2H), 2.44 (s, 3H), 1.85-1.75 (m, 2H), 1.68-1.59 (m, 2H), 1.33 (br, 1H). ^{13}C NMR ($CDCl_3$, 75 MHz): δ 156.3, 156.1, 152.5, 149.2, 149.0, 148.3, 148.3, 124.8, 124.8, 124.0, 122.2, 122.2, 121.5, 121.4, 62.6, 35.3, 32.4, 26.7, 21.3. HRMS (ESI): *m/z* calcd for $C_{15}H_{19}N_2O$ $[M+H]^+$ 243.1497; found 243.1492.

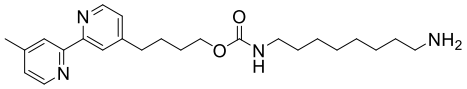

6

Compound 4. To a solution of 4-nitrophenyl chloroformate (0.21 g, 1.0 mmol) in dry CH_2Cl_2 (2 mL) was added dropwise a mixture of **5** (0.23 g, 0.95 mmol) and distilled DIEA (0.18 mL, 1.0 mmol) in CH_2Cl_2 (2 mL) via a syringe at 0 °C. After 3 h stirring at room temperature, the reaction mixture was added dropwise over a 30 min period to a solution of 1,8-diaminooctane (0.72 g, 5.0 mmol) in dry CH_2Cl_2 (100 mL) at 0 °C. Then the reaction mixture was allowed to proceed at room temperature for 12 h. The solution was washed with 1 N NaOH and brine several times, dried over Na_2SO_4. After filtration and concentration, the residual oil was purified by flash chromatography (SiO_2) eluting with MeOH/CH_2Cl_2/Et_3N (5:95:1 to 20:80:1, vol/vol/vol) to obtain product **6** as a white waxy solid (0.30 g, 78% yield). ^{1}H NMR ($CDCl_3$, 300 MHz): δ 8.56 (d, *J*(H, H) = 4.8, 1H), 8.53 (d, *J*(H, H) = 4.8, 1H), 8.22 (s, 1H), 8.22 (s, 1H), 7.14 (d, *J*(H, H) = 4.8, 1H), 7.14 (d, *J*(H, H) = 4.8, 1H), 4.76 (br, 1H), 4.09 (t, *J*(H, H) = 6.0, 2H), 3.17-3.11 (m, 2H), 2.75-32.65 (m, 4H), 2.44 (s, 3H), 1.86 (br, 2H), 1.80-1.70 (m, 2H), 1.68-1.64 (m, 2H), 1.46-1.44 (m, 4H), 1.28 (br, 8H). ^{13}C NMR ($CDCl_3$, 75 MHz): δ 156.8, 156.3, 156.2, 152.3, 149.2, 149.1, 148.4, 124.8, 124.1, 122.2, 121.4, 64.5, 42.1, 41.1, 35.1, 33.4, 30.1, 29.5, 29.3, 28.8, 26.9, 21.3. HRMS (ESI): *m/z* calcd for $C_{24}H_{37}N_4O_2$ $[M+H]^+$ 413.2917; found 413.2906.

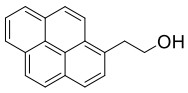

7

1-pyreneethanol 7. To a stirred suspension of lithium aluminium hydride ($LiAlH_4$) (0.38 g, 10 mmol) in dry THF (5 mL) was added a solution of 1-pyreneacetic acid (0.52 g, 2 mmol) in THF (5 mL) at 0 °C, then the resulting mixture was stirred at room temperature for 6 h. The reaction mixture was quenched by 1 N NaOH with ice-cooling bath. The THF layer was separated and dried over Na_2SO_4. After concentration, the residue was purified by flash chromatography (SiO_2) eluting with EtOAc/CH_2Cl_2 (10:90, vol/vol) to obtain product **6** as a light yellow solid (0.45 g, 92% yield). ^{1}H NMR ($CDCl_3$, 300

MHz): δ 8.33 (d, *J*(H, H) = 9.3, 1H), 8.20-8.12 (m, 4H), 8.05-7.98 (m, 3H), 7.94 (d, *J*(H, H) = 7.8, 1H), 4.14 (t, *J*(H, H) = 6.6, 2H), 3.66 (t, *J*(H, H) = 6.6, 2H), 1.45 (br, 1H) . ^{13}C NMR ($CDCl_3$, 75 MHz): δ 132.5, 131.5, 130.9, 130.4, 129.3, 128.0, 127.7, 127.5, 127.1, 126.0, 125.2, 125.2, 125.0, 124.9, 123.3, 63.9, 26.7. HRMS (ESI): *m/z* calcd for $C_{18}H_{15}O$ $[M+H]^+$ 247.1123; found 247.1116.

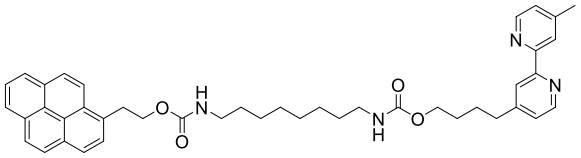

2

Guest 2. To a solution of 4-nitrophenyl chloroformate (0.15 g, 0.76 mmol) in chloroform (2 mL) was added dropwise a mixture of **7** (0.17 g, 0.69 mmol) and distilled DIEA (0.26 mL, 1.5 mmol) in chloroform (2 mL) via a syringe at 0 °C. After 3 h stirring at room temperature, the reaction mixture was added to a mixture of **6** (0.32 g, 0.76 mmol) and distilled DIEA (0.26 mL, 1.5 mmol) in chloroform (5 mL) at room temperature. Then the reaction mixture was refluxed for 24 h. The solution was washed with 1 N NaOH and brine several times, dried over Na_2SO_4. After filtration and concentration, the residual oil was purified by flash chromatography (SiO_2) eluting with EtOAc /CH_2Cl_2 (20:80 to 80:20, vol/vol) to obtain product **2** as a white solid (0.30 g, 65% yield).^{1}H NMR ($CDCl_3$, 300 MHz): δ 8.58-8.55 (m, 2H), 8.41 (d, *J*(H, H) = 9.3, 1H), 8.26 (s, 1H), 8.22 (s, 1H), 8.22-8.15 (m, 4H), 8.07-8.01 (m, 3H), 7.95 (d, *J*(H, H) = 7.8, 1H), 7.17-7.15 (m, 2H), 4.72 (br, 1H), 4.55 (t, *J*(H, H) = 7.2, 2H), 4.13 (t, *J*(H, H) = 6.0, 2H), 3.74 (t, *J*(H, H) = 7.2, 2H), 3.20-3.18 (m, 4H), 2.78 (t, *J*(H, H) = 7.5, 2H), 2.47 (s, 3H), 1.86-1.78 (m, 2H), 1.76-1.68 (m, 2H), 1.48 (br, 4H), 1.30 (br, 8H). ^{13}C NMR ($CDCl_3$, 75 MHz): δ 156.8, 156.7, 156.3, 156.1, 152.3, 149.2, 149.0, 148.3, 132.1, 131.5, 131.0, 130.4, 129.5, 127.9, 127.7, 127.6, 127.1, 126.0, 125.1, 125.0, 125.0, 124.8, 124.0, 123.4, 122.2, 121.4, 65.4, 64.2, 41.1, 35.1, 33.4, 30.1, 29.2, 28.8, 26.8, 26.7, 21.3. HRMS (ESI): *m/z* calcd for $C_{43}H_{49}N_4O_4$ $[M+H]^+$ 685.3754; found 685.3743.

Complex 1. Guest **2** (0.040 g, 0.058 mmol) was added to a solution of cis-dichlorobis(2,2'-bipyridine)ruthenium(II) dihydrate (0.030 g, 0.058 mmol) in methanol (3 mL), and the resulting mixture was heated for 18h at reflux. After cooling to room temperature, an excess of NH_4PF_6 was added as a saturated aqueous solution and stirring was continued for 30 min. The solvent was removed and the crude product was washed with water (70 mL). The orange solid was collected and purified by chromatography (alumina), eluting with acetonitrile/toluene (2:1, vol/vol). The complex was further purified through chromatography (SiO_2), eluting with acetonitrile/water /$KNO_{3\,(sat.\,aq.)}$ (95:4.9:0.1 vol/vol/vol), the product was collected and the solvent was removed. The solid was solubilized in small quantity of acetonitrile and filtered with a syringe filter, the solution was collected and the solvent was removed, to obtain **1** as a red solid (0.042 g, 52% yield). ^{1}H NMR (CD_3CN, 400 MHz): *δ* 8.50-8.48 (m, 4H), 8.43-8.38 (m, 3H), 8.24 (d, *J*(H, H) = 7.5 Hz, 2H), 8.21-8.17 (m, 2H), 8.11 (s, 2H), 8.06-7.97 (m, 6H), 7.73-7.71 (m, 4H), 7.54 (d,

J(H, H) = 5.8 Hz, 1H), 7.52 (d, *J*(H, H) = 5.8 Hz, 1H), 7.40-7.36 (m, 4H), 7.22-7.21 (m, 2H), 5.57 (br, 1H), 5.51 (br, 1H), 4.42 (t, *J*(H, H) = 6.5 Hz, 2H), 4.01 (t, *J*(H, H) = 6.3 Hz, 2H), 3.65 (t, *J*(H, H) = 6.8 Hz, 2H), 3.02-2.99 (m, 4H), 2.80 (t, *J*(H, H) = 7.3 Hz, 2H), 2.51 (s, 3H), 1.74 (m, 2H), 1.64 (m, 2H), 1.37 (m, 4H), 1.29 (br, 8H). ^{13}C NMR (CD_3CN, 100 MHz): δ 157.03, 156.69, 156.63, 156.50, 154.36, 151.65, 151.49, 150.91, 150.70, 150.41, 137.58, 132.9, 131.36, 130.86, 130.17, 129.22, 128.25, 127.56, 127.52, 127.47, 127.41, 126.87, 126.19, 125.07, 125.04, 124.92, 124.91, 124.65, 124.27, 124.19, 123.59, 64.75, 63.61, 40.46, 34.16, 32.84, 29.54, 28.78, 28.27, 26.24, 26.04, 20.25. HRMS (ESI): *m/z* calcd for $C_{63}H_{64}N_8O_4Ru^{2+}$ 549.20415; found 549.2063.

^{1}H Nuclear Magnetic Resonance studies

NMR spectra were recorded on 3 different NMR spectrometers: (1) an Avance II NMR spectrometer (Bruker Biospin) with a vertical 7.05 T narrow-bore/ultrashield magnet operating at 300 MHz for 1H observation and 75 MHz for ^{13}C observation by means of a 5-mm direct BBO H/X probe with Z gradient capabilities; (2) an Avance 400 NMR spectrometer (Bruker Biospin) with a vertical 9.4 T narrow-bore/ultrashield magnet operating at 400 MHz for ^{1}H observation by means of a 5-mm direct QNP ^{1}H/^{13}C/^{31}P/^{19}F probe with gradient capabilities; (3) an Avance III NMR spectrometer (Bruker Biospin) with a vertical 16.45 T narrow-bore/ultrashield magnet operating at 700 MHz for 1H observation by means of a 5-mm TXI ^{1}H/^{13}C/^{15}N probe with Z gradient capabilities. Chemical shifts are reported in parts per million (ppm, δ) relative to the ^{1}H residual signal of the deuterated solvent used. ^{1}H NMR splitting patterns with observed first-order coupling are designated as singlet (s), doublet (d), triplet (t), or quartet (q). Coupling constants (*J*) are reported in hertz. Data processing was performed with Topspin 2.0 software. Samples were not degassed. $CDCl_3$ from Eurisotop was used after filtration through an alumina pad followed by a distillation over calcium hydride.

Titration studies

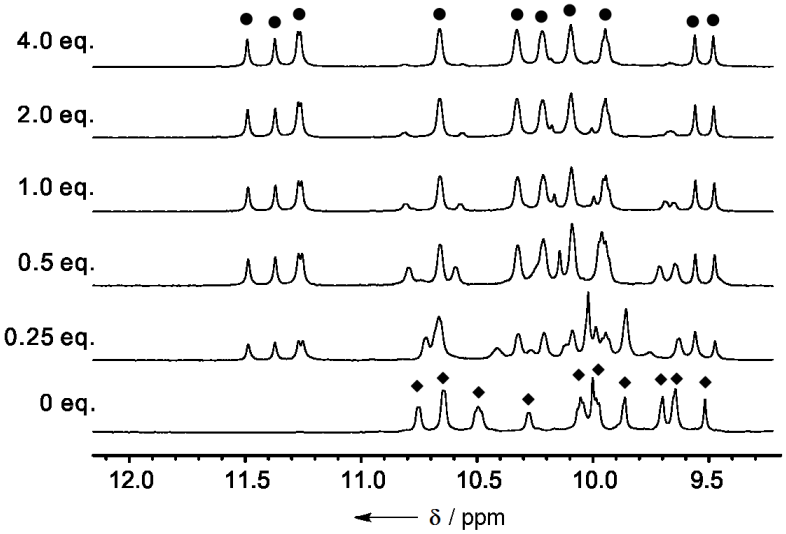

Figure S1. Representative 300 MHz NMR spectra of **4** (4 mM) in $CDCl_3$ titrated with **2**. Amide signals of the free double helix and foldaxane are marked with diamonds and black circles, respectively. K_{ass} = 1760 L mol^{-1}.

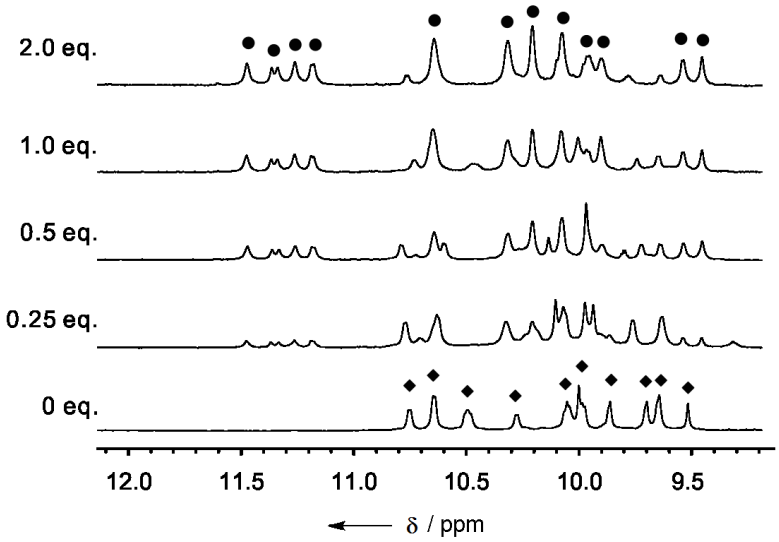

Figure S2. Representative 300 MHz NMR spectra of **4** (4 mM) in $CDCl_3$ titrated with **1**. Amide signals of the free double helix and foldaxane are marked with diamonds and black circles, respectively. K_{ass} = 1700 L mol^{-1}.

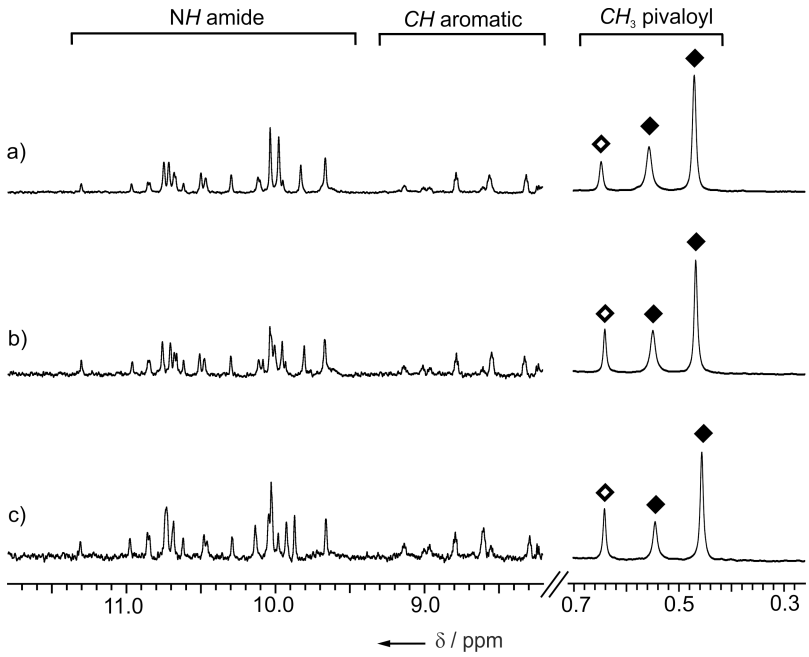

Figure S3. Partial 700 MHz ^{1}H NMR spectra of **4** at various concentrations in $CDCl_3$ at 298 K: a) 0.5 mM; b) 0.25 mM c) 0.125 mM. Empty and black diamonds indicate a single helix or a double helix configuration, respectively. Dimerization constant was calculated based on the pivaloyl integral using the following equation: $K_{dim} = [(\mathbf{4})_2] / [\mathbf{4}]^2$. K_{dim} was found to be 59000 L mol^{-1} at 298 K.

Determination of complex formation kinetics

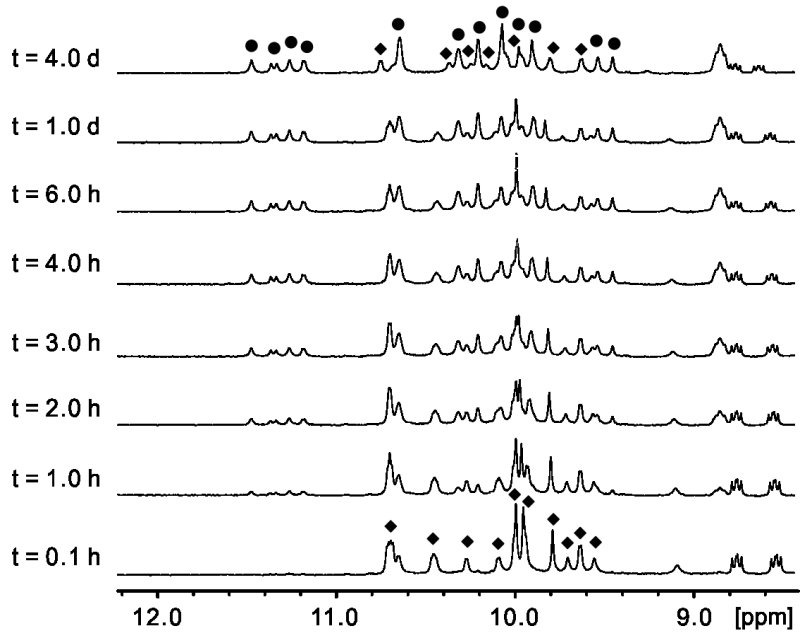

Figure S4. Excerpts of the ^{1}H NMR spectra (300 MHz) showing the formation of host-guest complexes **1**⊂(**4**)$_2$ from a mixture of host **4** (4 mM) and guest **1** (2 mM) in $CDCl_3$ at 25°C. The selected window presents the amide resonances as a function of time. Amide signals of host-guest complex are marked with black circles whereas free double helices of (**4**)$_2$ are marked with diamonds respectively.

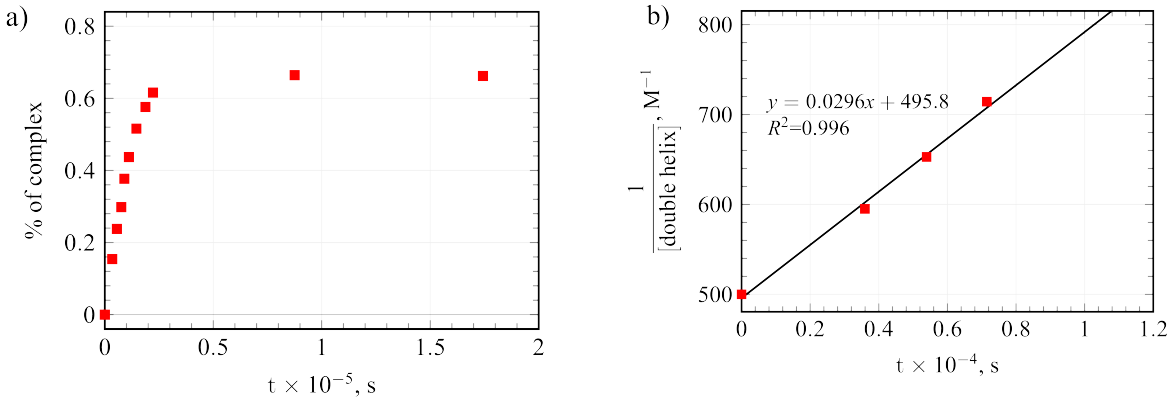

Figure S5. a) Timetraces of the formation of complexes **1**⊂(**4**)$_2$ from double stranded oligomer (**4**)$_2$ (2 mM) and rod **1** (2 mM) in $CDCl_3$ monitored by ^{1}H NMR at 298 K. b) Assuming that second order kinetics are valid during this initial phase (negligible reverse reaction), a second order kinetic constant can be calculated from the slope of the earliest data point (graph b) and was found to be $k = 0.0296$ s^{-1} M^{-1}. The half-life of a second order kinetic reaction in the case of $[\mathbf{1}]_{init} = [(\mathbf{4})_2]_{init}$ can be defined as $T_{1/2} = 1 / k [A]_{init}$ where $[\mathbf{A}]_{init} = [\mathbf{1}]_{init} = [(\mathbf{4})_2]_{init}$. From there, the lifetime of the reaction is $\tau = T_{1/2} / \ln 2$. In our case $T_{1/2} = 281$ min and $\tau = 406$ min.

Crystallographic studies

Tiny prism shaped crystals of $(\mathbf{4})_2$ and $\mathbf{2}\subset(\mathbf{4})_2$ were obtained from slow diffusion of n-hexane into chloroform.

Diffraction data for compound $(\mathbf{4})_2$ were measured on a Rigaku High flux FRX rotating anode equipped with an AFC partial chi goniometer and a Hybrid Pilatus 200K detector at the copper $K\alpha_1$ edge.

Diffraction intensities from crystal of $\mathbf{2}\subset(\mathbf{4})_2$ were measured on a Rigaku MM007 HF X-ray generator equipped with an AFC partial chi goniometer and a R-AXIS SPIDER image plate (IP) at the copper $K\alpha_1$ edge. The CrystalClear-SM Expert 2.1 b43 suite was used to integrate and reduce the data.

Both structures were solved with SHELXT and refined with SHELXL.[4] Full-matrix least-squares refinement were performed on F^2 for all unique reflections, minimizing $w(Fo^2 - Fc^2)^3$, with anisotropic displacement parameters for non-hydrogen atoms. All H atoms found in difference electron-density maps were refined freely, all the other were treated as riding on their parent C or N atoms. Data statistics are reported in the Tables S1 and S2 and cif files.

Both structures were containing disordered solvent molecules ($CHCl_3$) so the SQUEEZE procedure of the PLATON program[5] was used. The number of electrons and related VOID are reported in the cif files.

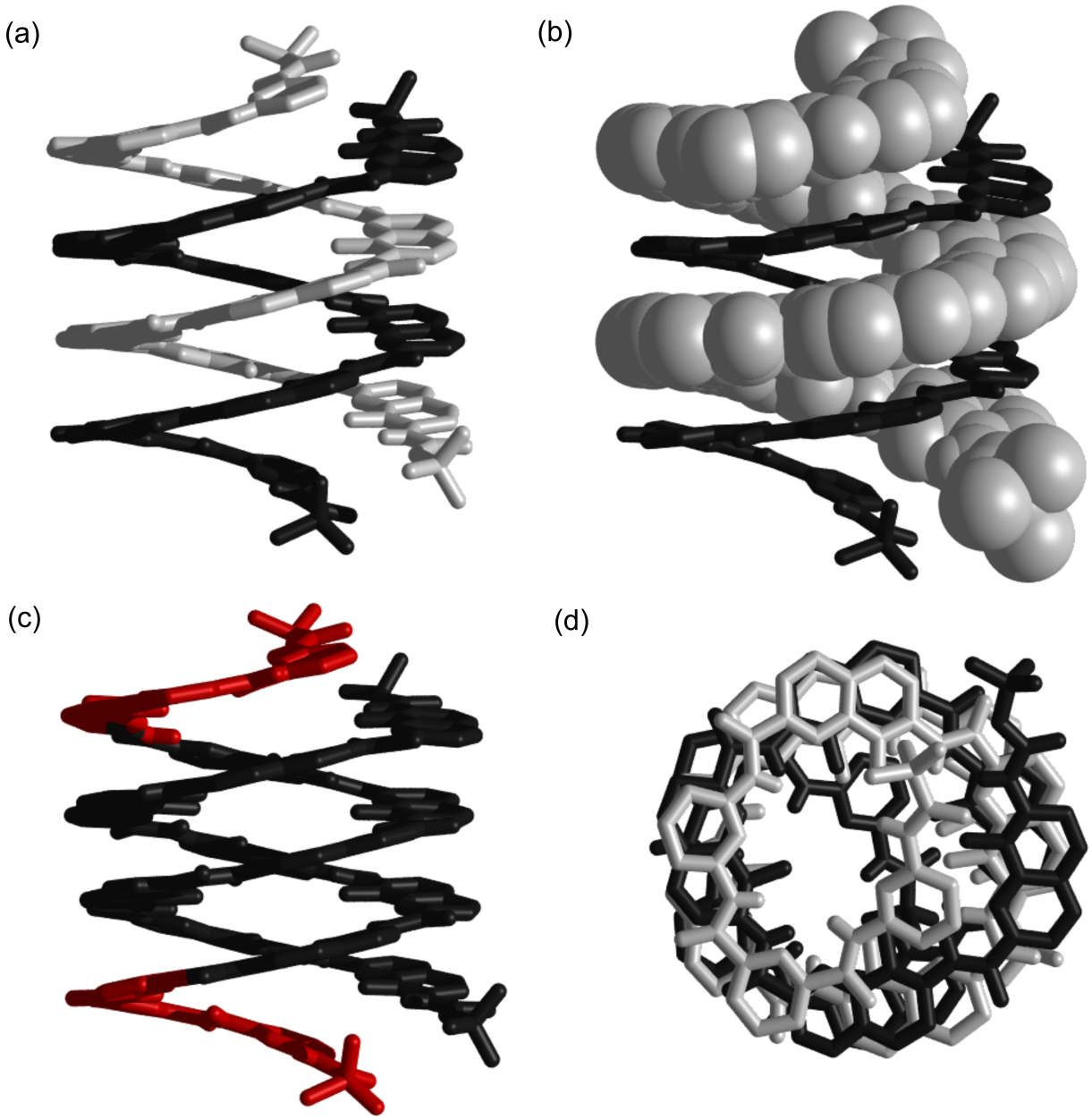

Figure S6. Side view of the crystal structure of $(\mathbf{4})_2$ in: (a) black and white tube representation and (b) tube and CPK representation. (c) Side view showing the anti-parallel configuration of the double helix in tube representation, each type of monomer being color-coded: pyridine (P) and fluoroquinoline (Q^F) are shown in red and black, respectively. (d) Top view of the double helix. Isobutoxy side chains and included solvent molecules are omitted for clarity. Only the polar hydrogens are shown.

Table S1: Crystal data and structure refinement for double helix $(\mathbf{4})_2$

CCDC 1418615	
Crystal Data	
Formula	C110 H108 F6 N20 O17, 2(CHCl3)
Formula Weight	2334.91
Crystal System	orthorhombic
Space group	Pnna (No.52)
Cell paramters a, b, c [Angstrom]	45.001(5) 23.593(7) 25.085(4)
Cell angles alpha, beta, gamma [deg]	90 90 90
V [$Å^3$]	26633(9)
Z	8
D(calc) [g/cm^3]	1.165
Mu(CuKα) [/mm]	1.778
F(000)	9712
Crystal Size [mm]	0.05 x 0.10 x 0.20
Data Collection	
Temperature (K)	130
Radiation [Angstrom]	CuKα 1.54178
Theta Min-Max [Deg]	2.6, 49.7
Dataset	-38: 44 ; -23: 15 ; -23:23
Tot., Uniq. Data, R(int)	39817, 12099, 0.087
Observed Data [I > 2.0 sigma(I)]	7389
Refinement	
Nref, Npar	12099,1465
R, wR2, S $w = 2(FO^2)+(0.2000P)^2]$ where $P=(FO^2+2FC^2)/3$	0.1483, 0.3867,1.45
Max. and Av. Shift/Error	0.49,0.01
Min. and Max. Resd. Dens. [$e^-/Å^3$]	-0.35,0.48

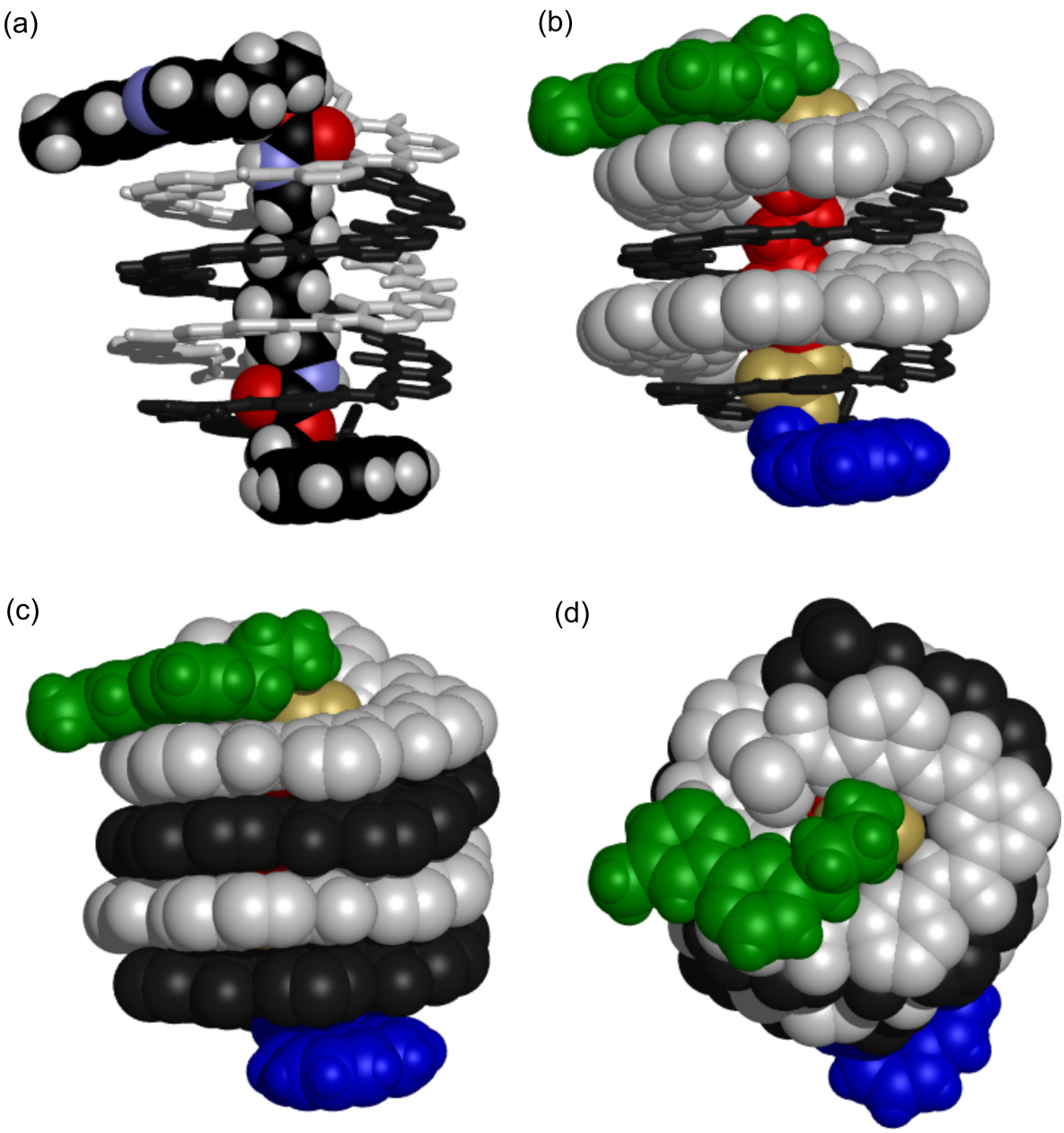

Figure S7. Side view of the crystal structure of **1**⊂(**4**)$_2$ in: (a) black and white tube and CPK representation for the double helix and the rod, respectively. In (b), (c) and (d) the rod is shown in CPK representation and the bipyridine, the xylene, the carbamate function and the alkyl segment are shown in green, blue, gold and red colour, respectively. In (c) the double helix is shown in tube and CPK representation whereas in (d) it appears completely as CPK representation. (d) Top view of the foldaxane. Isobutoxy side chains and included solvent molecules are omitted for clarity. Only the polar hydrogens are shown.

Table S2: Crystal data and structure refinement for double helix **1**⊂(**4**)$_2$

CCDC 1418616	
Crystal Data	
Formula	C137.5 H137.5 Cl15 F6 N21.5 O18.5
Formula Weight	3032.93
Crystal System	triclinic
Space group	P-1 (No. 2)
Cell paramters a, b, c [Angstrom]	20.2500(14) 29.674(2) 30.922(2)
Cell angles alpha, beta, gamma [deg]	99.704(7) 98.045(7) 106.601(7)
V [Å^3]	17200(2)
Z	2
D(calc) [g/cm^3]	1.172
Mu(CuKα) [/mm]	2.755
F(000)	6282
Crystal Size [mm]	0.04 x 0.10 x 0.10
Data Collection	
Temperature (K)	130
Radiation [Angstrom]	CuKα 1.54178
Theta Min-Max [Deg]	6.6, 45.5
Dataset	-18: 18 ; -27: 27 ; -28:28
Tot., Uniq. Data, R(int)	108525, 28337, 0.113
Observed Data [I > 2.0 sigma(I)]	10794
Refinement	
Nref, Npar	28337,3604
R, wR2, S w = 2(FO^2)+(0.2000P)^2] where P=(FO^2+2FC^2)/3	0.1213, 0.3418,0.93
Max. and Av. Shift/Error	0.11,0.01
Min. and Max. Resd. Dens. [e$^-$/Å^3]	-0.42,0.82

Threading $1\subset(4)_2$

Monitoring the threading process was conducted as follows: solutions of **4** were prepared in $CDCl_3$ (the $CDCl_3$ was purified from trace amounts of protons and water traces by passing through predried (300 °C) $Al_2O_{3\ basic}$ 100 μm powder at 4 mM and 80 μM concentrations, respectively. Double-helix $(\mathbf{4})_2$ was prepared by dimerization of **4**, one day before the experiment, which was sufficient for full dimerization of **4** to be accomplished, resulting in $(\mathbf{4})_2$ formation (2 mM). After 24 h, when the process of $(\mathbf{4})_2$ formation was finished:

1. the given quantity of **1** solution was transferred into a spectroscopic quartz cuvette;
2. solvent was evaporated and a predetermined volume of $(\mathbf{4})_2$ solution was added into this cell, thus solubilizing **1**;
3. obtained solution was frozen at liquid nitrogen temperature (77 K) for further degassing by multiple freeze-pump-thaw cycles, afterwards the cell is blowtorch sealed.

Solutions with different molar ratios between **1** and dimer $(\mathbf{4})_2$: 1:6, 1:12, 1:32 were studied.

UV-vis absorption and emission spectra

Electronic absorption spectra were recorded on a spectrophotometer Cary 5G UV-Vis-NIR (Varian) using 10 and 1 mm synthetic quartz (Suprasil) quartz cells. Luminescence: fluorescence and phosphorescence at temperatures 77 K and 295 K) spectra were recorded on a Fluorolog-3 (Jobin Yvon) spectrophotometer with iHR-320 spectrograph (range 280 – 1500 nm with grating 1200 gr/mm, blazed at 500 nm) and photomultipliers from Hamamatsu Photonics: R928 (range 280 – 900 nm).

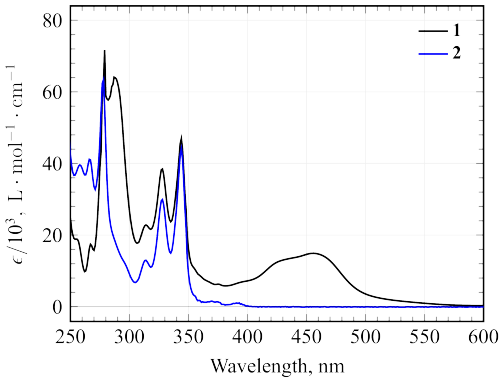

Figure S8. Electronic absorption spectra of **1** and **2** in $CDCl_3$.

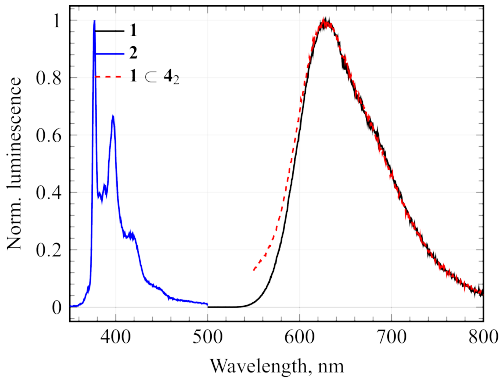

Figure S9. Luminescence spectra of **1**, $\mathbf{1}\subset(\mathbf{4})_2$ (λ_{exc} = 440 nm) and **2** (λ_{exc} = 355 nm) in $CDCl_3$.

Quantum yields

Fluorescence quantum yield studies were performed using a Fluorolog-3 (Jobin Yvon) spectrofluorometer with iHR-320 (range 280 – 1500 nm with grating 1200 gr/mm, blazed at 500 nm) and photomultipliers from Hamamatsu Photonics: R928 (range 280 – 900 nm) and determined versus standard of known quantum yield, $[Ru(bpy)_3]^{2+}$ (bpy = 2,2'–bipyridine) in non-degassed H_2O - 0.028.[6] All spectra were recorded as an average of 5 scans and corrected for instrumental sensitivity.

Table S3. Photophysical properties of free thread **1** and **1**⊂(**4**)$_2$ in $CDCl_3$.

	$\lambda_{em.max}$	Φ_{degas} [a]	τ, μ [b]	$K_{eq.}$
1	620	0.077(0.008)	2.5	5±1
1⊂(**4**)$_2$	620	0.05(0.02)	1.2	-

[a] Φ_{em} $CDCl_3$ solution cf. $[Ru(bpy)_3]^{2+}$ in H_2O. Values in parentheses in air-equilibrated solution.
[b] MLCT luminescence lifetime in dilute degassed $CDCl_3$.

Time-resolved measurements

The transient absorption / time-resolved luminescence set-up was built as follows (Figure): a frequency tripled Nd:YAG amplified laser system (30 ps, 30 mJ @1064 nm, 20 Hz, Ekspla model PL 2143) output was used to pump an optical parametric generator (Ekspla model PG 401) producing tunable excitation pulses in the range 410 – 2300 nm. The residual fundamental laser radiation was focused in a high pressure Xe filled breakdown cell where a white light pulse for sample probing was produced. All light signals were analyzed by a spectrograph (Princeton Instruments Acton model SP2300) coupled with a high dynamic range streak camera (Hamamatsu C7700, 1ns-1ms). Accumulated sequences (sample emission, probe without and with excitation) of pulses were recorded and treated by HPDTA (Hamamatsu) software to produce two-dimensional maps (wavelength *vs* delay) of transient absorption intensity in the range 300 – 800 nm. Typical measurement error was better than 10^{-3} O. D. Data were analysed using home-made software developed in LabVIEW 2014 system-design platform and development environment. The trust-region dogleg algorith[7] (supported by LabVIEW 2014) was applied to determine the set of parameters that best fit the set of input data. The trust-region dogleg algorithm was used instead of Levenberg-Marquardt algorithm, the latter being less stable in most cases during optimization process, because trust region methods are robust, and can be applied to ill-conditioned problems.

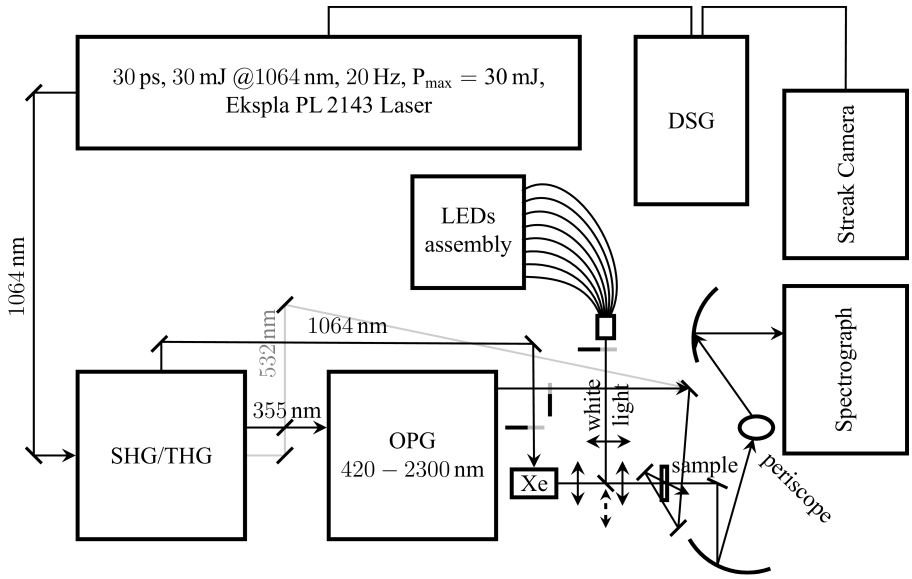

Figure S10. Scheme for sub-nanosecond laser set-up; SHG/THG – second/third harmonic generator, OPG – optical parametric generator, LED – light emitting diode, DSG – digital signal generator.

The emission lifetime τ of **1** lies in the range of 1 − 2.6 µs, this fact caused us to work in a 10 µs timescale. The streak-camera in this timescale is triggered by the rising edge of laser pulse train, causing a ~1 µs jitter. To suppress the effect of such a big jitter on the emission decays, we recorded every time-resolved 2D-emission map after every laser excitation pulse (20 Hz). Jitter-correction was applied to every 2D-map: all 2D-maps were aligned by rising edge of emission, after that the maps were integrated and averaged. The emission decays at 630 nm were analysed at different times during the complexation process between **1** and $(\mathbf{4})_2$.

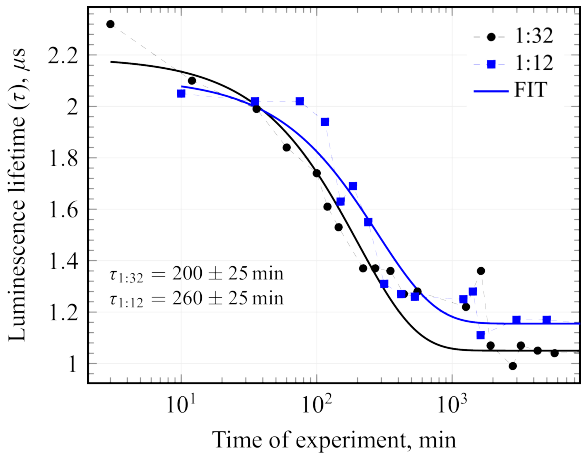

Figure S11. Real time threading denoted by changes in observed luminescence lifetime considering a monoexponential decay.

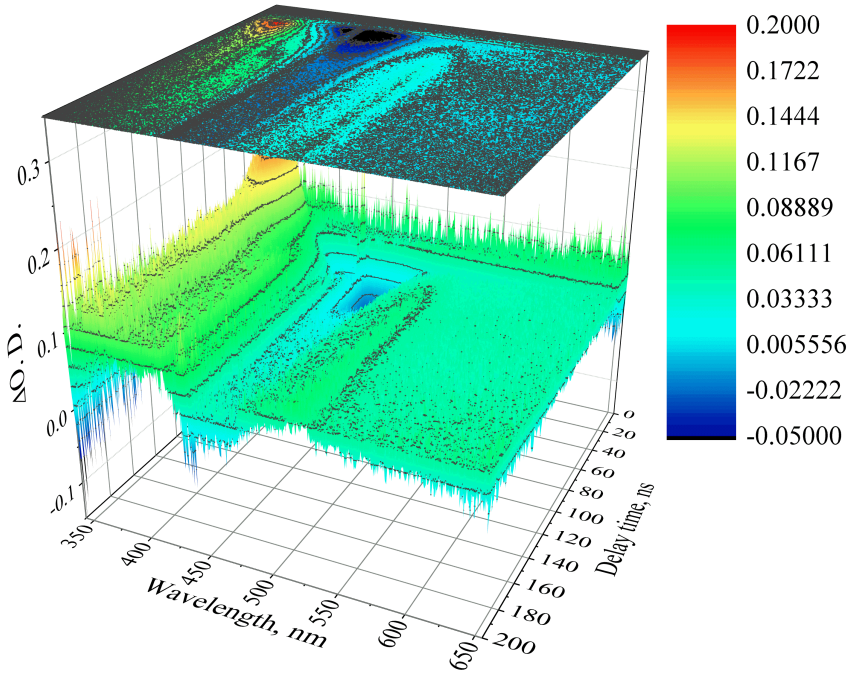

Figure S12. Transient absorption map of **1** in $CDCl_3$ (λ_{exc} = 440 nm).

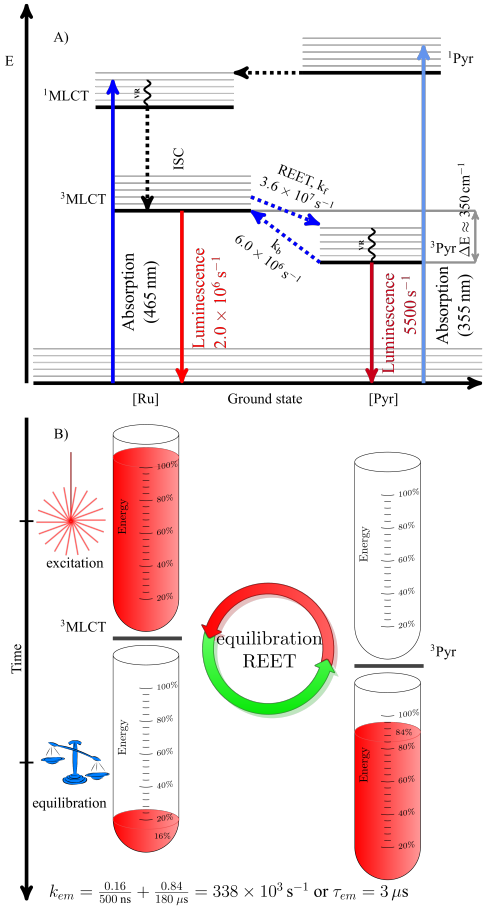

Figure S13. A) Perrin-Jablonski diagram showing pertinent energy levels of bichromophore and kinetics of REET and delayed luminescence of **1. B**) Representation of energy redistribution between ^{3}MLCT and triplet pyrene states following selective MLCT excitation.

Distribution of Intercomponent Distances in 1

Pyrene energy reservoir in **1** is connected to $Ru(bpy)_3^{2+}$ moiety via a long flexible chain. Due to Brownian motion and bond rotation, the distance between the two choromphores is constantly changing. To determine the average interchromophore, the approach described by Lakowicz[8] could be used. The nonlinear analysis of the pyrene fluorescence decay monitored at 410 nm (see Figure S13) should be accomplished. Pyrene fluorescence is quenched in the presence of ruthenium containing unit due to energy transfer from pyrene to a ^{1}MLCT state. Assuming that the interchromophore distance could be described as a Gaussian function:

$$f(d_{da}) = \frac{1}{\sigma\sqrt{2\pi}} e^{\left(-0.5\left(\frac{d-\mu}{\sigma}\right)^2\right)} \qquad (1),$$

in this equation μ is the most likely distance and σ represents the width of the distribution, then fluorescence decay of the pyrene undergoing intramolecular quenching by the $Ru(bpy)_3^{2+}$ ^{1}MLCT state can be described by:

$$I(t) = A\int_0^\infty f(d_{da}) e^{\left(-\frac{t}{\tau_d}\left(\frac{R_0}{d_{da}}\right)^6\right)} dd_{da} \qquad (2),$$

where A is a preexponential factor, R_0 (taken as 21 Å, according to Barrigelletti and Ward[9]) is the critical transfer radius, and τ_d is the lifetime (150 ns) of the unquenched singlet pyrene state in ACN. Analysis of $I(t)$ according to eq. 2 gives μ = 10 Å and σ = 2 Å, the halfwidth of distribution is given by 2.35 σ = 4.7 Å.

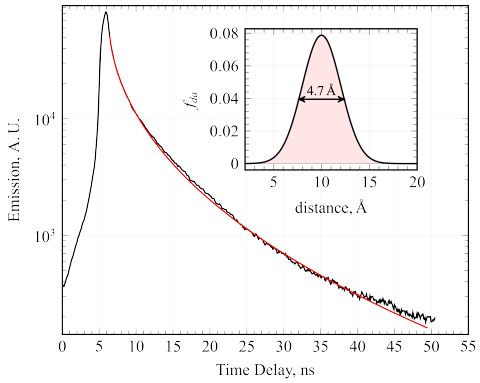

Figure S14. Time-resolved decay of pyrene emission fit (λ_{em} = 410 nm, ACN, black), according to equation 2 (λ_{exc} = 355 nm).

NMR spectra

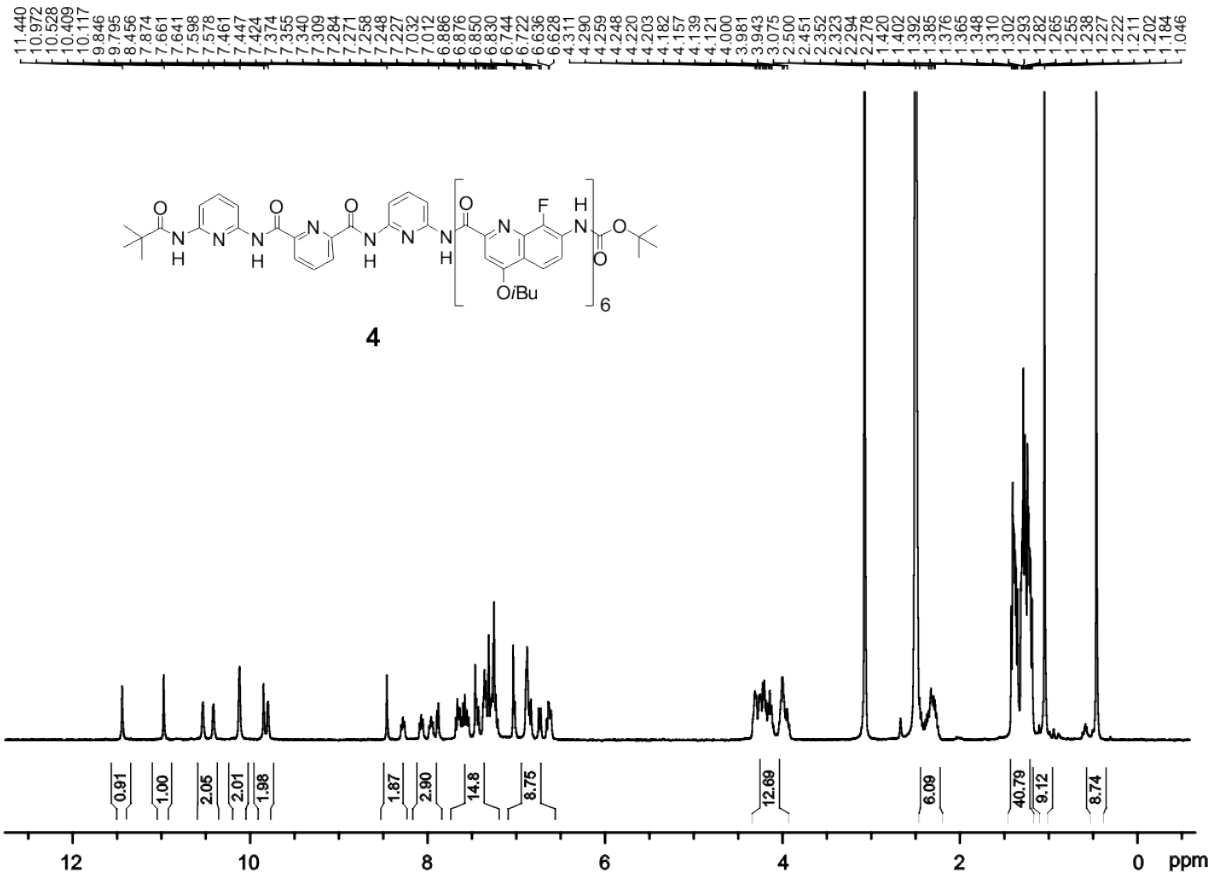
11.440
10.972
10.528
10.409
10.117
9.846
9.795
8.456
7.874
7.661
7.641
7.598
7.578
7.461
7.447
7.424
7.374
7.355
7.340
7.309
7.284
7.271
7.258
7.248
7.227
7.032
7.012
6.886
6.876
6.850
6.830
6.744
6.722
6.636
6.628
4.311
4.290
4.259
4.248
4.220
4.203
4.182
4.157
4.139
4.121
4.000
3.981
3.943
3.075
2.500
2.451
2.352
2.323
2.294
2.278
1.420
1.402
1.392
1.385
1.376
1.365
1.348
1.310
1.302
1.293
1.282
1.265
1.255
1.238
1.227
1.222
1.211
1.202
1.184
1.046
O/Bu
6
4
0.91
1.00
2.05
2.01
1.98
1.87
2.90
14.8
8.75
12.69
6.09
40.79
9.12
8.74
12
10
8
6
4
2
0
ppm

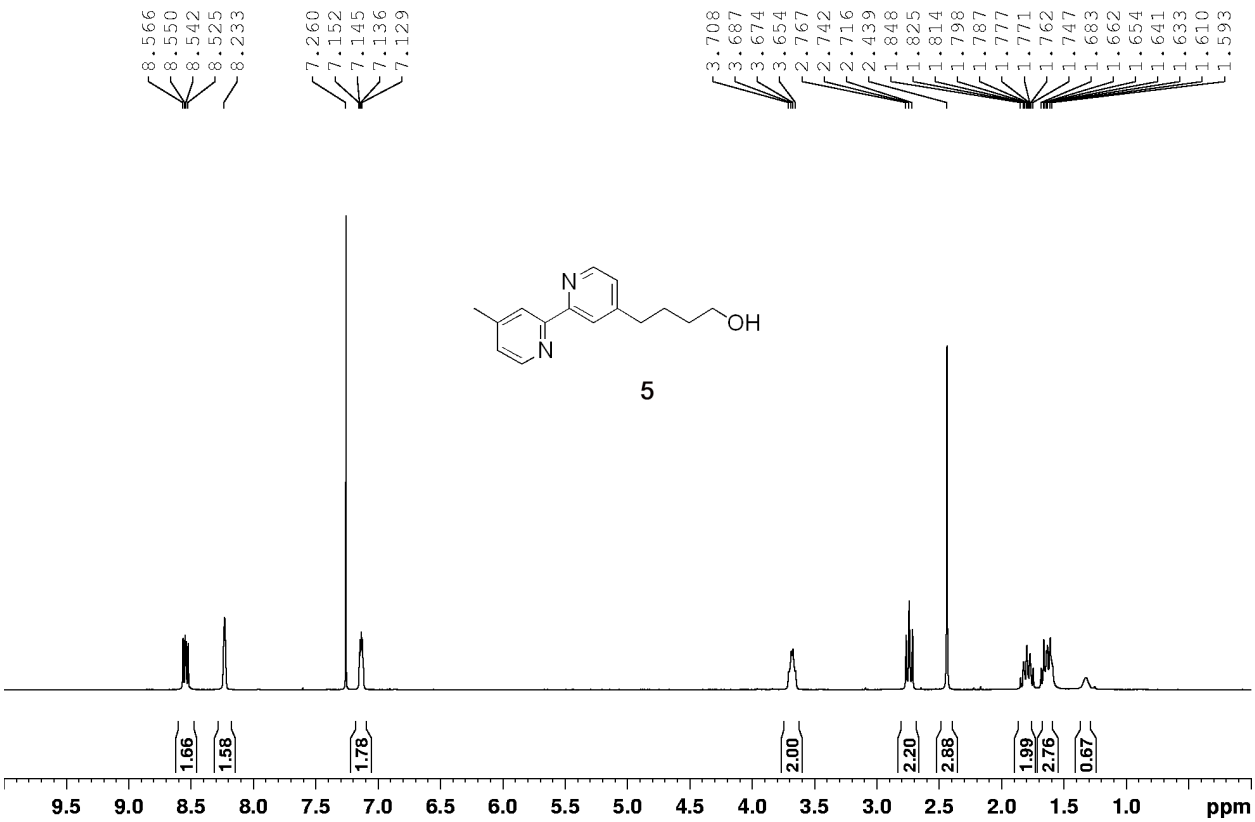
8.566
8.550
8.542
8.525
8.233
7.260
7.152
7.145
7.136
7.129
3.708
3.687
3.674
3.654
2.767
2.742
2.716
2.439
1.848
1.825
1.814
1.798
1.787
1.777
1.771
1.762
1.747
1.683
1.662
1.654
1.641
1.633
1.610
1.593
N
OH
N
5
1.66
1.58
1.78
2.00
2.20
2.88
1.99
2.76
0.67
9.5
9.0
8.5
8.0
7.5
7.0
6.5
6.0
5.5
5.0
4.5
4.0
3.5
3.0
2.5
2.0
1.5
1.0
ppm

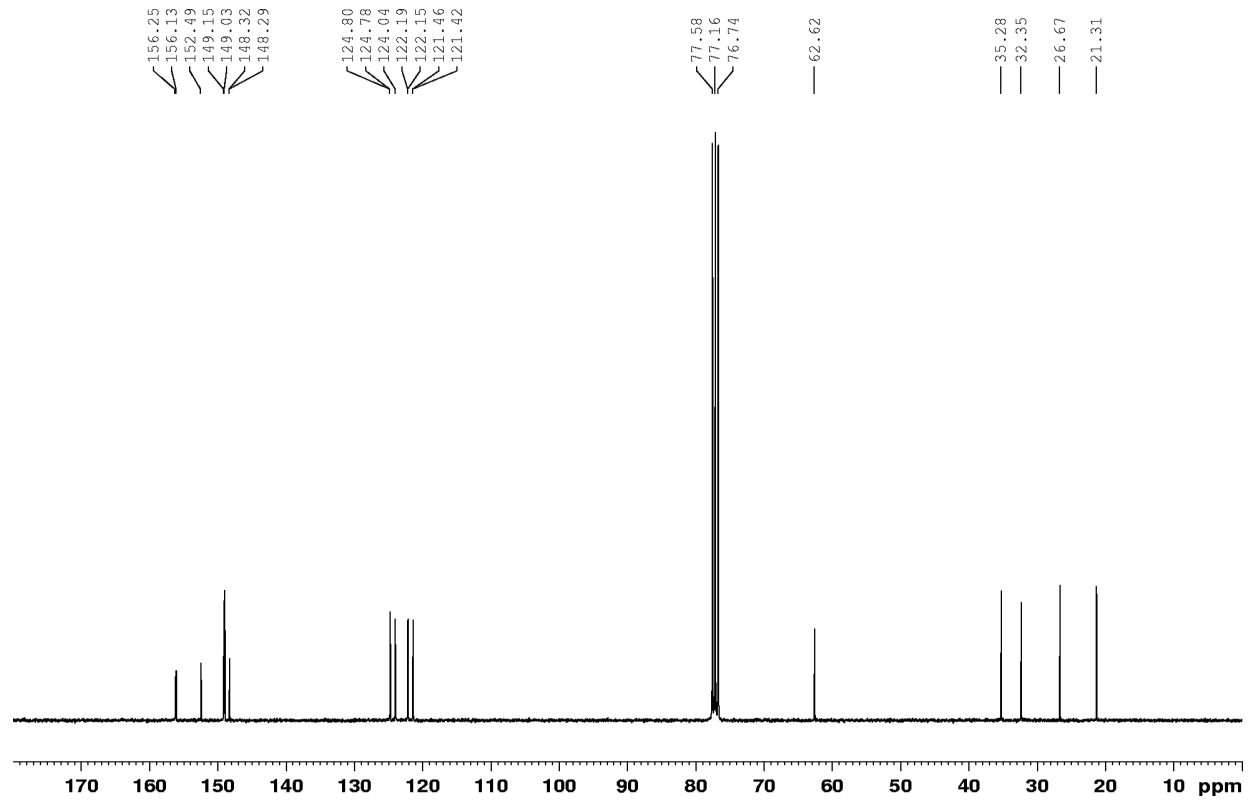
156.25
156.13
152.49
149.15
149.03
148.32
148.29
124.80
124.78
124.04
122.19
122.15
121.46
121.42
77.58
77.16
76.74
62.62
35.28
32.35
26.67
21.31
170
160
150
140
130
120
110
100
90
80
70
60
50
40
30
20
10
ppm

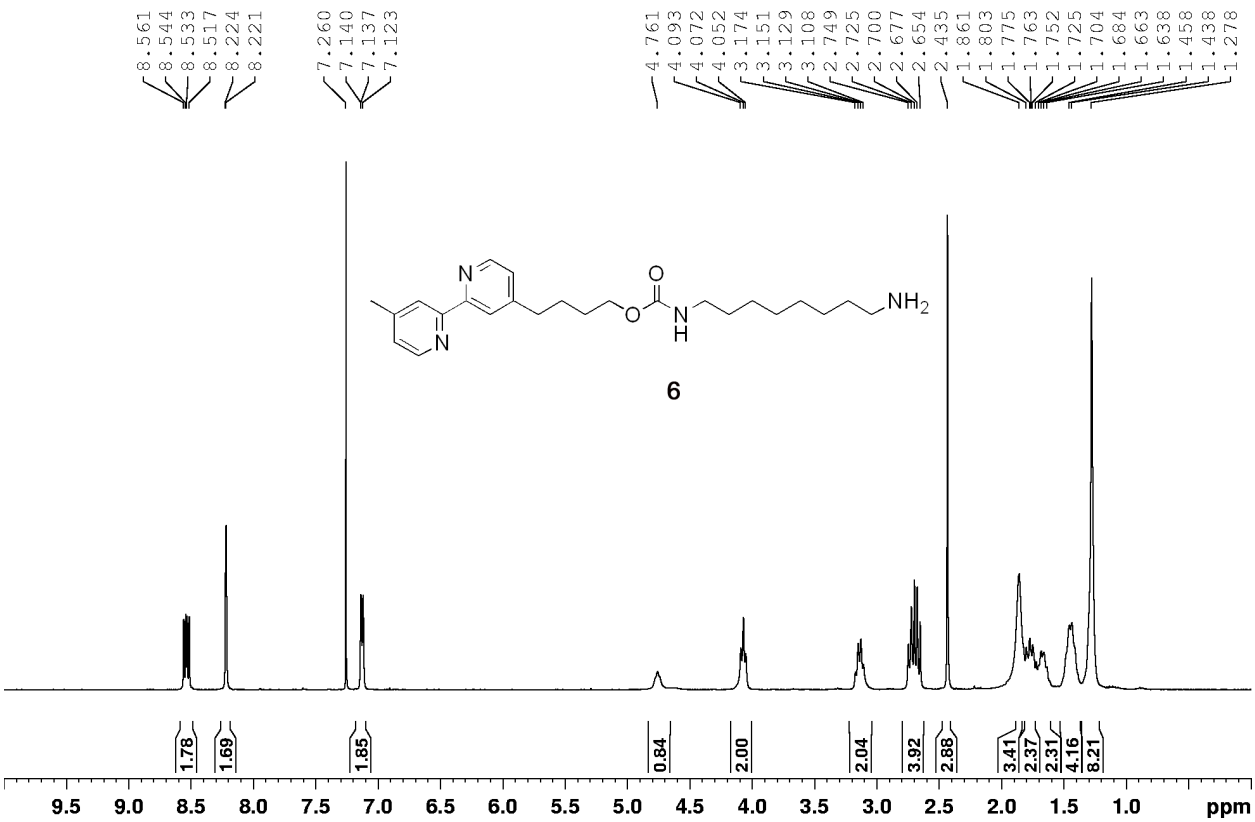
8.561
8.544
8.533
8.517
8.224
8.221
7.260
7.140
7.137
7.123
4.761
4.093
4.072
4.052
3.174
3.151
3.129
3.108
2.749
2.725
2.700
2.677
2.654
2.435
1.861
1.803
1.775
1.763
1.752
1.725
1.704
1.684
1.663
1.638
1.458
1.438
1.278
N
O
O
N
H
NH2
N
6
1.78
1.69
1.85
0.84
2.00
2.04
3.92
2.88
3.41
2.37
2.31
4.16
8.21
9.5 9.0 8.5 8.0 7.5 7.0 6.5 6.0 5.5 5.0 4.5 4.0 3.5 3.0 2.5 2.0 1.5 1.0 ppm

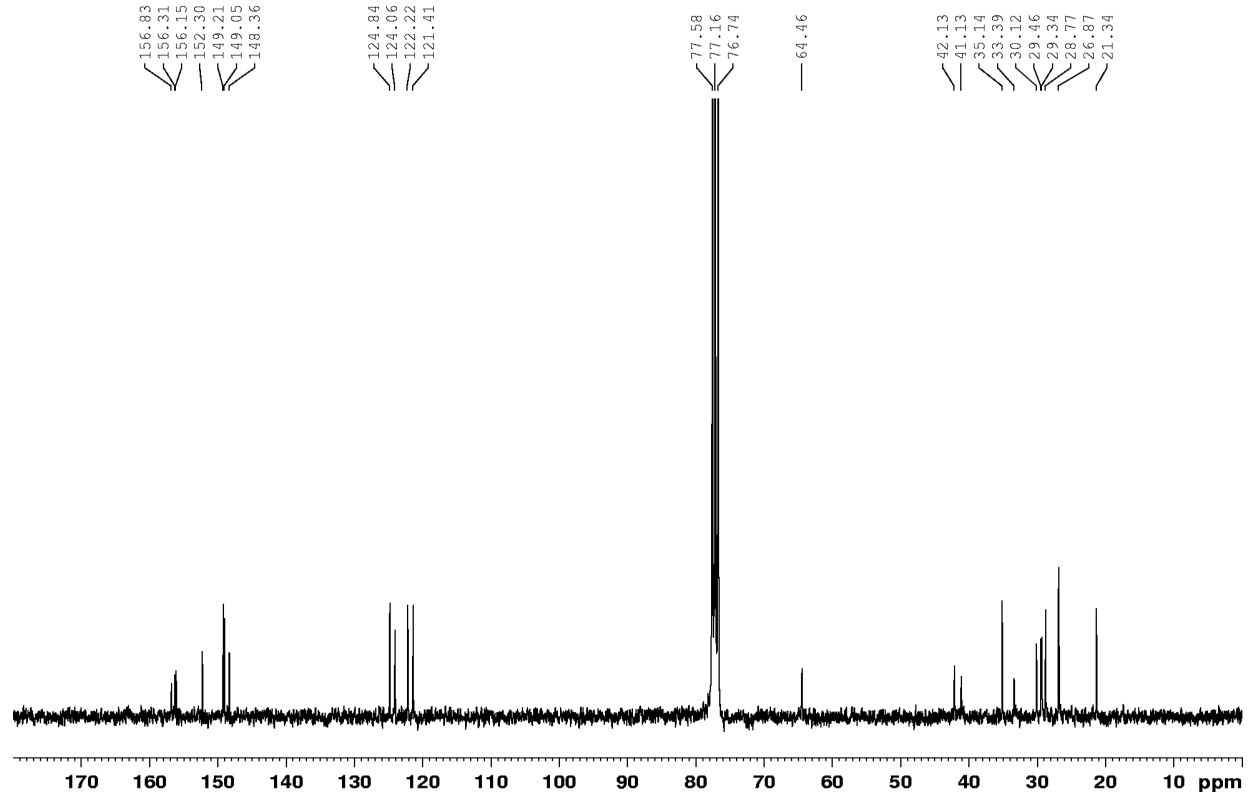
156.83
156.31
156.15
152.30
149.21
149.05
148.36
124.84
124.06
122.22
121.41
77.58
77.16
76.74
64.46
42.13
41.13
35.14
33.39
30.12
29.46
29.34
28.77
26.87
21.34
170 160 150 140 130 120 110 100 90 80 70 60 50 40 30 20 10 ppm

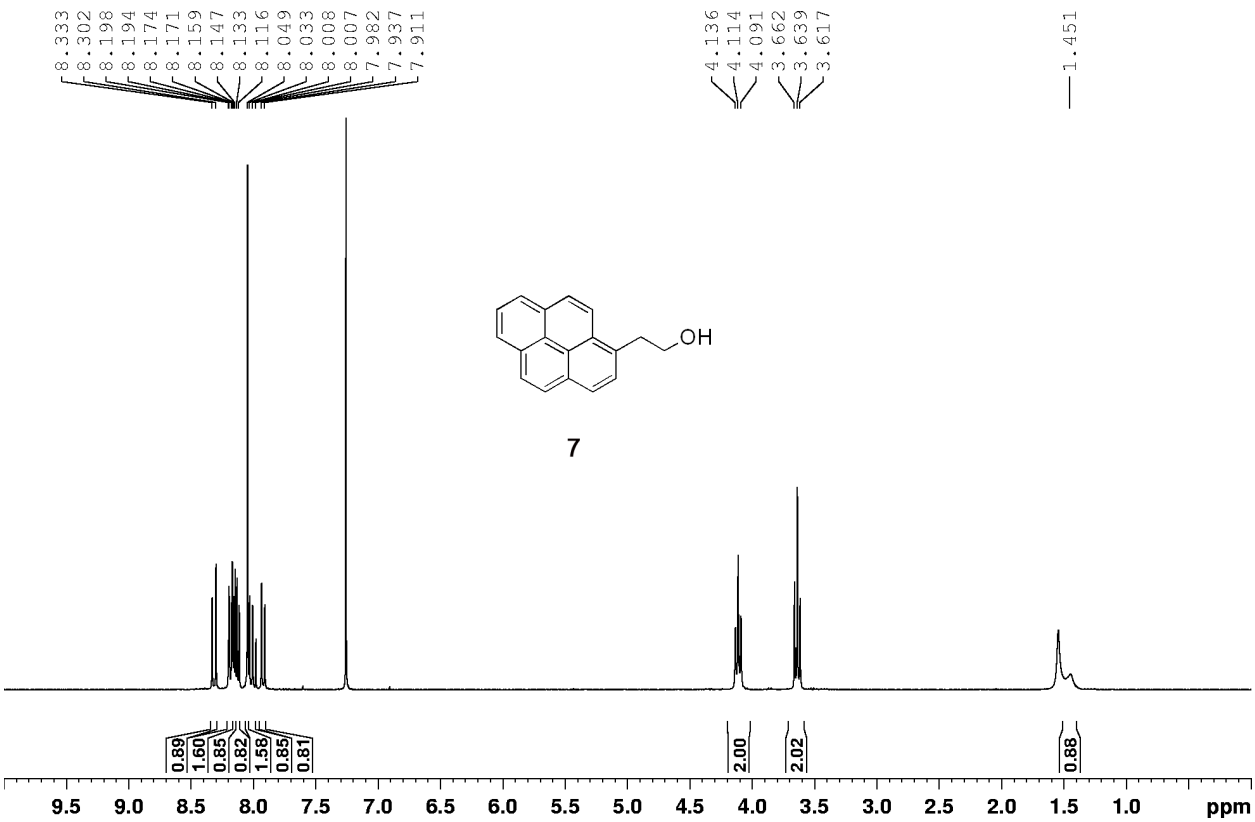
8.333
8.302
8.198
8.194
8.174
8.171
8.159
8.147
8.133
8.116
8.049
8.033
8.008
8.007
7.982
7.937
7.911
4.136
4.114
4.091
3.662
3.639
3.617
1.451
OH
7
0.89
1.60
0.85
0.82
1.58
0.85
0.81
2.00
2.02
0.88
9.5
9.0
8.5
8.0
7.5
7.0
6.5
6.0
5.5
5.0
4.5
4.0
3.5
3.0
2.5
2.0
1.5
1.0
ppm

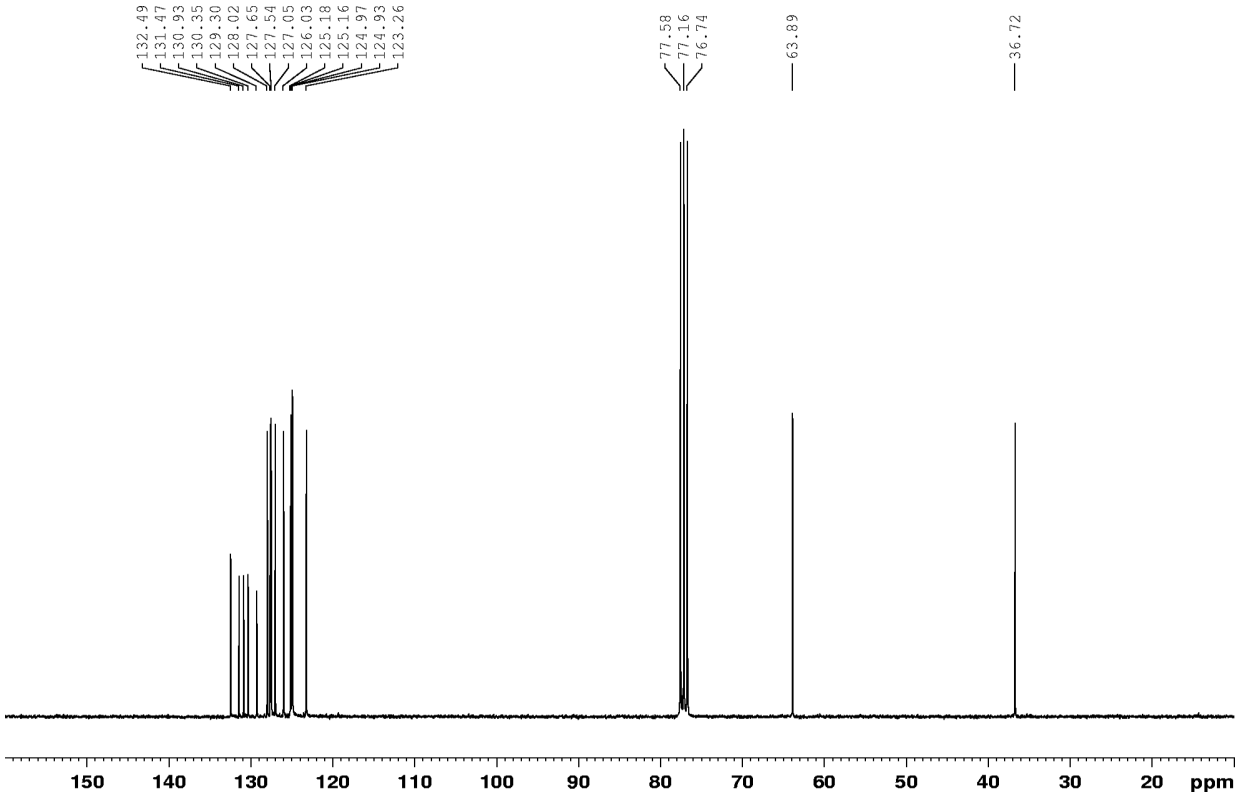
132.49
131.47
130.93
130.35
129.30
128.02
127.65
127.54
127.05
126.03
125.18
125.16
124.97
124.93
123.26
77.58
77.16
76.74
63.89
36.72
150
140
130
120
110
100
90
80
70
60
50
40
30
20
ppm

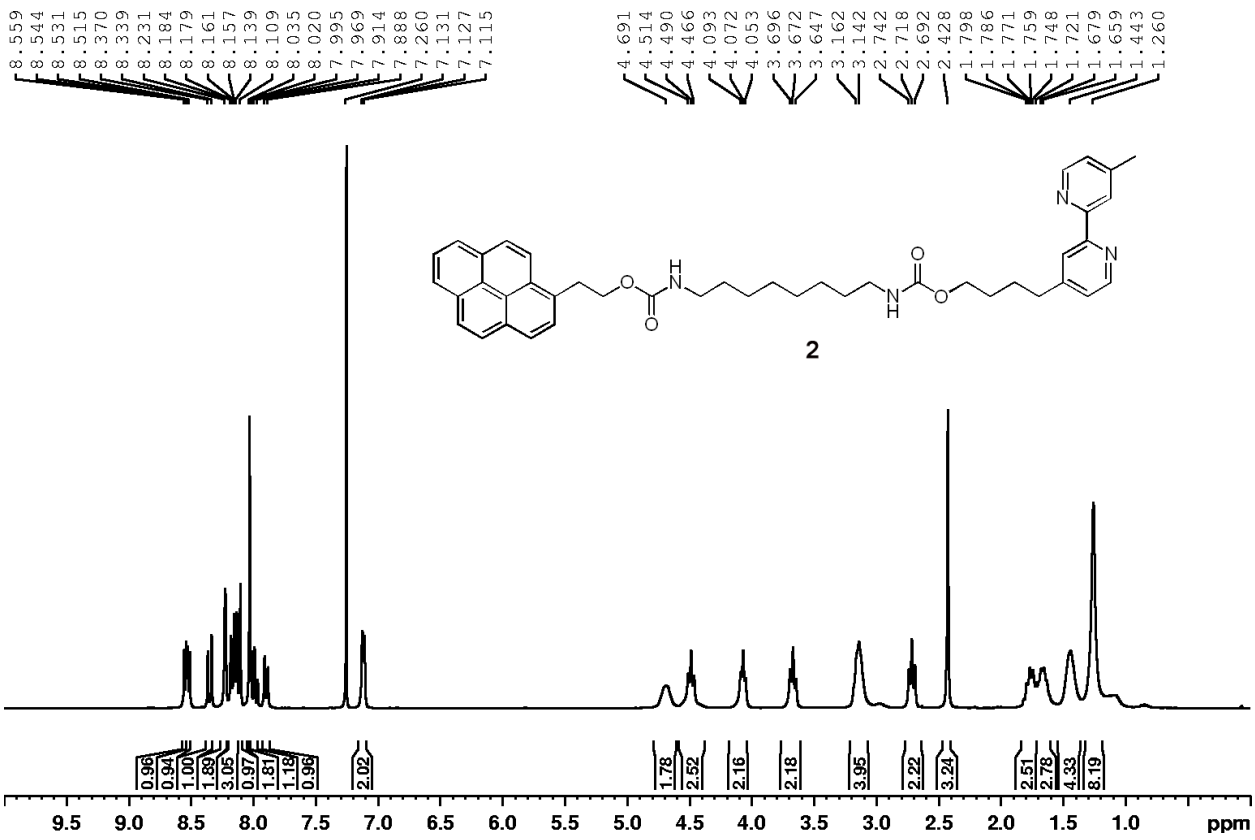
8.559
8.544
8.531
8.515
8.370
8.339
8.231
8.184
8.179
8.161
8.157
8.139
8.109
8.035
8.020
7.995
7.969
7.914
7.888
7.260
7.131
7.127
7.115
4.691
4.514
4.490
4.466
4.093
4.072
4.053
3.696
3.672
3.647
3.162
3.142
2.742
2.718
2.692
2.428
1.798
1.786
1.771
1.759
1.748
1.721
1.679
1.659
1.443
1.260
2
0.96
0.94
1.00
1.89
3.05
0.97
1.81
1.19
0.96
2.02
1.78
2.52
2.16
2.18
3.95
2.22
3.24
2.51
2.78
4.33
8.19
9.5 9.0 8.5 8.0 7.5 7.0 6.5 6.0 5.5 5.0 4.5 4.0 3.5 3.0 2.5 2.0 1.5 1.0 ppm

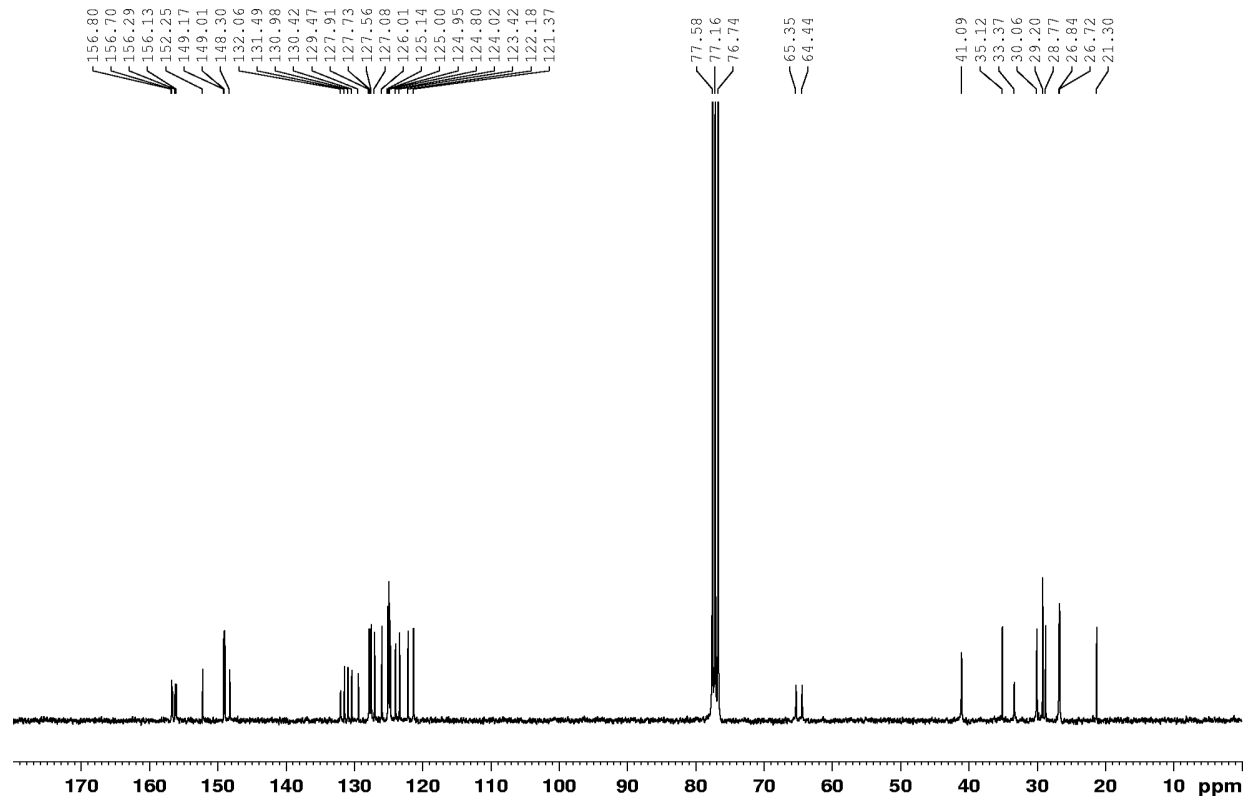
156.80
156.70
156.29
156.13
152.25
149.17
149.01
148.30
132.06
131.49
130.98
130.42
129.47
127.91
127.73
127.56
127.08
126.01
125.14
125.00
124.95
124.80
124.02
123.42
122.18
121.37
77.58
77.16
76.74
65.35
64.44
41.09
35.12
33.37
30.06
29.20
28.77
26.84
26.72
21.30
170 160 150 140 130 120 110 100 90 80 70 60 50 40 30 20 10 ppm

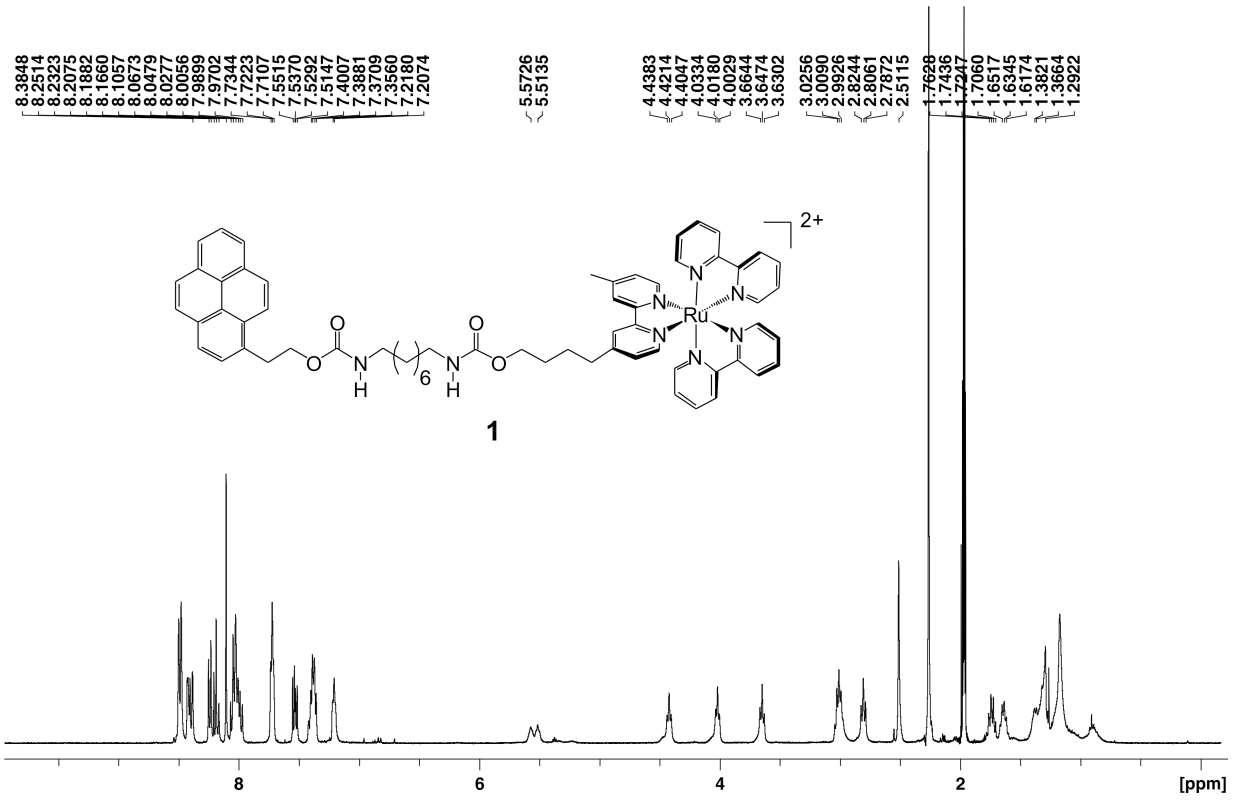
8.3848
8.2514
8.2323
8.2075
8.1882
8.1660
8.1057
8.0673
8.0479
8.0277
8.0056
7.9899
7.9702
7.7344
7.7223
7.7107
7.5515
7.5370
7.5292
7.5147
7.4007
7.3881
7.3709
7.3560
7.2180
7.2074
5.5726
5.5135
4.4383
4.4214
4.4047
4.0334
4.0180
4.0029
3.6644
3.6474
3.6302
3.0256
3.0090
2.9926
2.8244
2.8061
2.7872
2.5115
1.7628
1.7436
1.7247
1.7060
1.6517
1.6345
1.6174
1.3821
1.3664
1.2922
2+
Ru
N
O
H
6
1
8
6
4
2
[ppm]

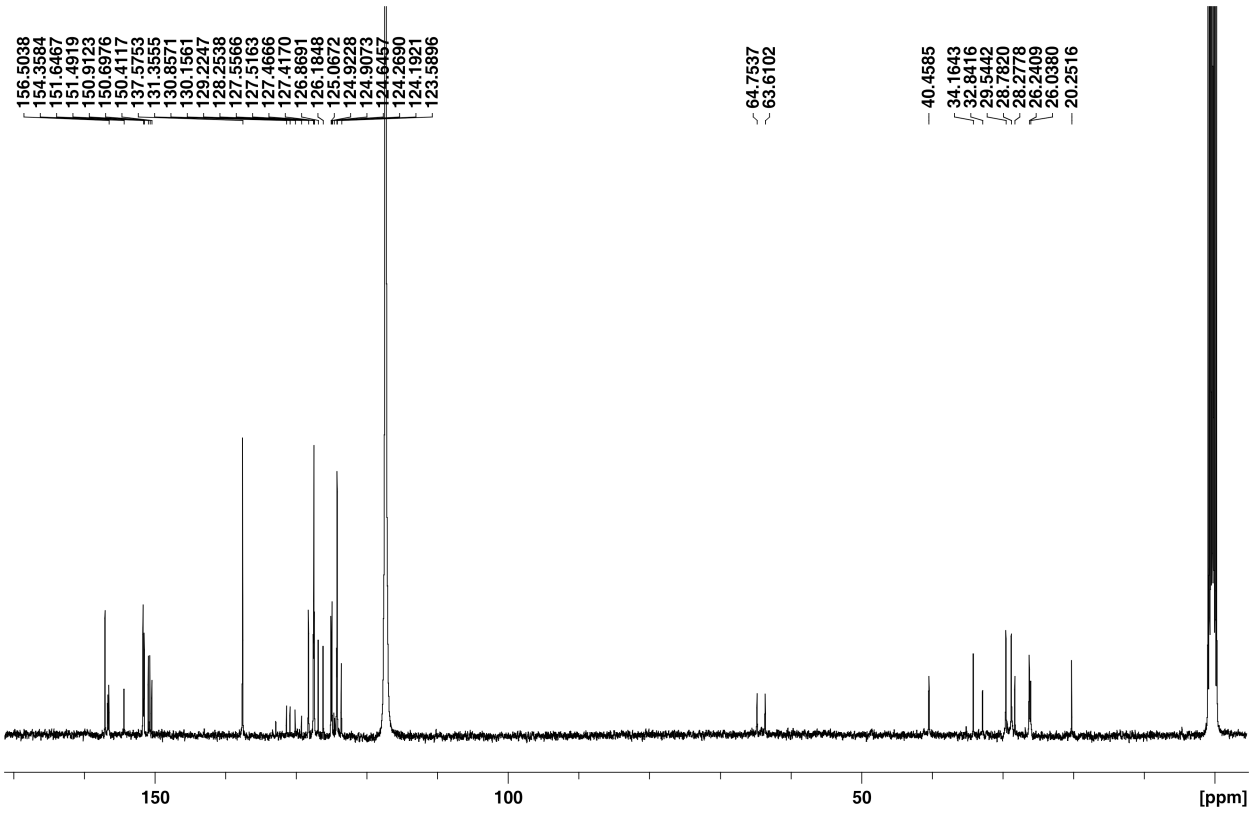
156.5038
154.3584
151.6467
151.4919
150.9123
150.6976
150.4117
137.5753
131.3555
130.8571
130.1561
129.2247
128.2538
127.5566
127.5163
127.4666
127.4170
126.8691
126.1848
125.0672
124.9228
124.9073
124.6457
124.2690
124.1921
123.5896
64.7537
63.6102
40.4585
34.1643
32.8416
29.5442
28.7820
28.2778
26.2409
26.0380
20.2516
150
100
50
[ppm]

References

[1] C. Bao, Q. Gan, B. Kauffmann, H. Jiang, I. Huc, A self-assembled foldamer capsule: combining single and double helical segments in one aromatic amide sequence *Chem. Eur. J.* **2009**, *15*, 11530.

[2] Q. Gan, C. Bao, B. Kauffmann, A. Grélard, J. Xiang, S. Liu, I. Huc, H. Jiang, Quadruple and double helices of 8-fluoroquinoline oligoamides. *Angew. Chem. Int. Ed.* **2008**, *47*, 1715.

[3] L. Della Ciana, I. Hamachi, T. J. Meyer, Synthesis of Side-Chain Derivatives of 2,2'-Bipyridine. *J. Org. Chem.* **1989**, *54*, 1731.

[4] Sheldrick, *Acta Cryst.* **2015**, A71, 3.

[5] A. L. Spek, *Acta Cryst.* **2009**, D65, 148.

[6] H. Ishida, S. Tobita, Y. Hasegawa, R. Katoh, K. Nozaki, Recent Advances in Instrumentation for Absolute Emission Quantum Yield Measurements. *Coord. Chem. Rev.* **2010**, *254*, 2449.

[7] M. L. A. Lourakis, A. A. Argyros, Is Levenberg-Marquardt the Most Efficient Optimization. Algorithm for Implementing Bundle Adjustment? In *Computer Vision, 2005. ICCV 2005. Tenth IEEE International Conference on*; **2005**; Vol. 2, pp. 1526.

[8] J. Lakowicz, *Principles of Fluorescence Spectroscopy*; Springer US, **2006**.

[9] A. F. Morales, G. Accorsi, N. Armaroli, F. Barigelletti, S. J. A. Pope, M. D. Ward, Interplay of Light Antenna and Excitation "Energy Reservoir" Effects in a Bichromophoric System Based on Ruthenium−Polypyridine and Pyrene Units Linked by a Long and Flexible Poly(ethylene Glycol) Chain. *Inorg. Chem.* **2002**, *41*, 6711.